DFT Models for Copper(II) Bispidine Complexes: Structures, Stabilities, Isomerism, Spin Distribution, and Spectroscopy

MIHAIL ATANASOV,[1,2] PETER COMBA,[1] BODO MARTIN,[1] VERA MÜLLER,[1] GOPALAN RAJARAMAN,[1] HEIDI ROHWER,[1] STEFFEN WUNDERLICH[1]

[1]*Universität Heidelberg, Anorganisch-Chemisches Institut, Im Neuenheimer Feld 270, D-69120 Heidelberg, Germany*

[2]*Institute of General and Inorganic Chemistry, Bulgarian Academy of Sciences, Bl. 11, 1113 Sofia, Bulgaria*

Received 16 November 2005; Accepted 19 January 2006
DOI 10.1002/jcc.20412
Published online in Wiley InterScience (www.interscience.wiley.com).

Abstract: Various DFT and *ab initio* methods, including B3LYP, HF, SORCI, and LF-density functional theory (DFT), are used to compute the structures, relative stabilities, spin density distributions, and spectroscopic properties (electronic and EPR) of the two possible isomers of the copper(II) complexes with derivatives of a rigid tetradentate bispidine ligand with two pyridine and two tertiary amine donors, and a chloride ion. The description of the bonding (covalency of the copper–ligand interactions) and the distribution of the unpaired electron strongly depend on the DFT functional used, specifically on the nonlocal DF correlation and the HF exchange. Various methods may be used to optimize the DFT method. Unfortunately, it appears that there is no general method for the accurate computation of copper(II) complexes, and the choice of method depends on the type of ligands and the structural type of the chromophore. Also, it appears that the choice of method strongly depends on the problem to be solved. LF-DFT and spectroscopically oriented CI methods (SORCI), provided a large enough reference space is chosen, yield accurate spectroscopic parameters; EDA may lead to a good understanding of relative stabilities; accurate spin density distributions are obtained by modification of the nuclear charge on copper; solvation models are needed for the accurate prediction of isomer distributions.

 J Comput Chem 27: 1263–1277, 2006

Key words: DFT models; copper(II) bispidine complexes; *ab initio* methods

Introduction

Density functional theory has become a common and useful tool for the prediction of structures and properties of transition metal compounds, and has found wide applications, particularly in bioinorganic chemistry, where, due to the size of the systems these problems are still inaccessible to *ab initio* theory.[1,2] Specifically for the reactivity of copper enzymes and corresponding low molecular weight model systems there exists an increasing number of recent mechanistic work based on density functional theory (DFT) calculations.[3–6] However, although the various DFT methods have been extensively tested, and their accuracy validated for organic and organometallic systems, for classical coordination and bioinorganic compounds, this has only been done for a limited number of systems.[5,7–11] It is common knowledge that pure DFT functionals give a bonding description that is too covalent,[3,7,12,13] specifically for copper(II) complexes, and for this reason hybrid functionals such as B3LYP[14] were introduced and found to give an improved but still not satisfactory description of the bonding interaction.[7,12] Functionals with varying amounts of HF exchange (between 0 and 50%) have been proposed, and are implemented in common programs. The B3LYP[14] and BP86[15] functionals are the most commonly used. However, the bonding description of copper(II) complexes with the B3LYP functional is still too covalent. Two different approaches to improve the DFT method were dis-

Correspondence to: P. Comba; e-mail: peter.comba@aci.uni-heidelberg.de

Contract/grant sponsor: the German Science Foundation (DFG)

Contract/grant sponsor: the Alexander von Humboldt Foundation (AvH, fellowship to G.R.)

This article contains Supplementary Material availalbe at http://www.interscience.wiley.com/jpages/0192-8651/suppmat

cussed for $[CuCl_4]^{2-}$,[7] where the accurate spin distribution is known from experiment,[16,17] and for $[Cu(dien)_2]^{2+}$ (dien = 3-azapentane-1,5-diamine), where observed structures and spectroscopic data could be used to tune and validate the functional.[18] In the former example, the amount of HF exchange and correlation were optimized,[7] while in the latter the nuclear charge of copper (Q = 29) was modified empirically to improve the agreement between experimental and computed structural and spectroscopic data.[18]

In our present study, we investigate the validity of the two approaches (variation of the amount of HF exchange and of the nuclear charge of the copper center) and also of the corresponding DFT methods with copper(II) bispidine complexes (mixed amine/pyridine donor set; see Chart 1 for a description of the ligands used and Fig. 1 for the single crystal X-ray structure of L^1).

Bispidine ligands are very rigid and complementary for copper(II).[19–21] They enforce square pyramidal or *cis*-octahedral coordination geometries with various forms of Jahn-Teller-type distortions,[21–24] and they form very stable 1:1 complexes[25,26] with the possibility to bind monodentate substrates in two distinctly different sites.[27] These are part of the reasons why copper–bispidine complexes are of interest in biomimetic chemistry and catalysis.[27–33]

For the validation of the two proposed schemes for the accurate prediction of structural and electronic data we employed a number of observables to which the functional and nuclear charge were fitted. These include structural data, isomer distributions, stability constants, spin distributions derived from experimentally determined EPR spectra, as well as electronic d–d transitions and EPR g- and A-tensor values.

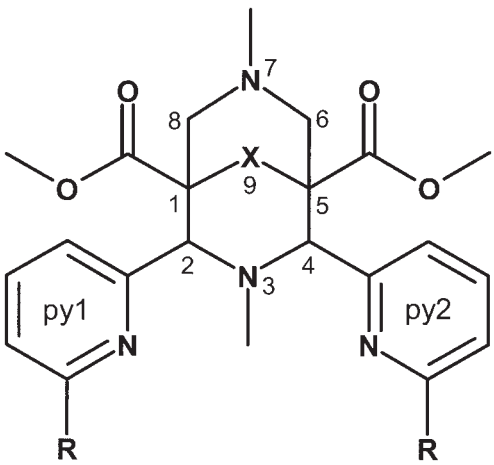

L^1: R=H **a: X=CO**

L^2: R=CH_3 **b: X=$C(OH)_2$**

Chart 1.

Figure 1. Plot of the experimentally determined molecular structure of L^{1a}.

Experimental Section

General and Measurements

The solvents and chemicals for spectroscopy were of the highest possible grade and used without further purification; solvents for EPR spectroscopy were degassed before use. $[Cu(L^{1b})(Cl)]Cl$ was prepared as described before[29] and fully characterized (C, H, N; UV-vis; IR; the electronic and EPR spectra were recorded with the hydrolyzed ligand L^{1b}). The elemental analysis were obtained from the analytical department of the chemical institutes of the University of Heidelberg.

Frozen solution EPR spectra of $[Cu(L^{1b})(Cl)]^+$ were measured at X-band frequency, using a Bruker ELEXSYS-E-500 spectrometer. Spectra in various solvent mixtures [MeCN, DMF/MeCN (2:1), DMF/MeOH (2:1) and DMF/H_2O (2:1)], Cu^{2+} complex concentrations (10, 5, and 1 μM), and concentrations of added Cl^- salt (tetrabutyl ammonium chloride at 25, 50, 100, and 250 μM concentrations) were qualitatively identical. The best resolution (see Fig. 2, in the Results and Discussion section) was obtained in DMF/MeOH with Cu^{2+} and Cl^- concentrations of 1 and 25 μM, respectively. The spectrum reported was recorded at a temperature of 116 K, with a microware frequency of 9.28 GHz. The spin-Hamiltonian parameters were obtained by simulation of the spectra with the XSophe simulation software (version 1.1.4).[34,35] The electronic spectrum reported was obtained at 25.0°C from an aqueous solution (concentration 5 mM), with a JASCO V-570 UV-vis-NIR spectrophotometer.

Computational Methods

General

A simplified model system for the bispidine ligands was used in all calculations, in which the ester side chains at C1 and C5 of the ligand backbone (see Chart 1) were replaced by H atoms. In the course of the synthesis, depending on experimental conditions, the carbonyl group at C9 of the bispidine backbone is hydrolyzed to a

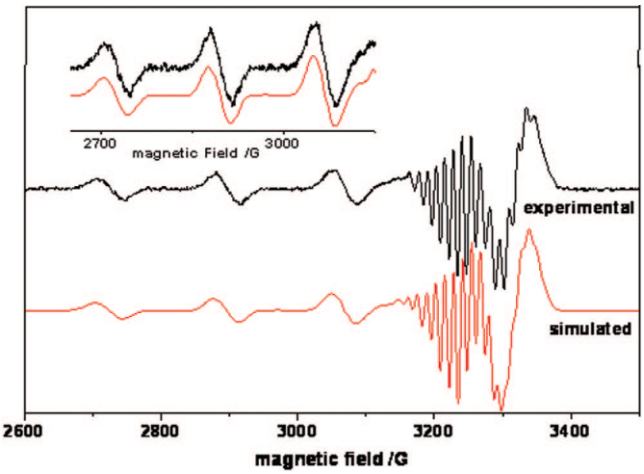

Figure 2. Second derivative experimental (frozen solution) and simulated EPR spectrum of $[Cu(L^{1b})(Cl)]^+$.

geminal diol.[27,29] It is known that a ketone at C9 decreases the nucleophilicity of the tertiary amines N3 and N7. Therefore, calculations were performed on compounds containing both the hydrolyzed and nonhydrolyzed forms of the ligand, to investigate the influence on the calculated spin densities.

DFT calculations were performed with the software packages Gaussian 03,[36] ORCA,[37,38] ADF,[39,40] and the LF-DFT[41] module based on the ADF program. Gaussian 03 was used for geometry optimizations, frequency calculations, and the spin density calibration of the functional. ORCA was used to calculate the EPR **g** and **A** tensor values. The electronic transitions were obtained with the Spectroscopically Oriented Configuration Interaction (SORCI) method.[37] ADF was used for geometry optimization and the energy decomposition analysis (EDA). The Ligand Field Density Functional Theory scheme (LF-DFT) was used to calculate electronic transitions and g-tensor components.

Optimized Structures, Energies, and Spin Densities

For the initial structure optimizations, Becke's three parameter hybrid exchange functional, in conjunction with the correlation functional of Lee, Yang, and Parr (B3LYP),[14] and a combination of the 6-31G basis set for hydrogen and the 6-311G(d) basis set for heavy atoms were used. Geometry optimizations were performed in the gas phase. Frequency calculations were performed on all optimized structures to verify their status as true minima on the potential energy surface and to obtain zero-point corrections to the energies.

Adjustment of the Functional

The effect of the functional on the relative energies, geometries, and spin densities was studied using a 6-31G(d) basis set and various current functionals; for details see Tables 4–6 in the Results and Discussion section below. All structures investigated have previously been shown to be minima on the potential energy surface and are given without zero-point or thermal corrections.

For the nonstandard functionals, the amount of density functional exchange and correlation was constructed from local as well as nonlocal density functional (DF) and local exchange, nonlocal DF correlation and HF exchange, according to eqs. (1) and (2) for BLYP and BP86, respectively, where $a = \% E_XHF/100$. For the functionals with the LYP correlation, the amount of nonlocal exchange was fixed at 0.72 (the experimentally calibrated value for B3LYP) and only the local exchange was varied, whereas for the BP86 functional both the nonlocal and local DF exchange were varied, in analogy to a similar recent study on $CuCl_4$.[7]

$$E_{XC}(BLYP) = E_CLSDA + 0.72\Delta E_XB88 + aE_XHF + (1-a)E_XLSDA + 0.81\Delta E_CLYP \quad (1)$$

$$E_{XC}(BP86) = E_CLSDA + (1-a)\Delta E_XB88 + aE_XHF + (1-a)E_XLSDA + \Delta E_CP86. \quad (2)$$

Spin densities were calculated with the Mulliken Population Analysis[42] (MPA) approach. The Natural Population Analysis (NPA)[43] and Atoms in Molecules (AIM)[44] methods were not used, as they have been shown to give comparable results to the MPA scheme.[7] The overall simplicity of the computational setup is justified because the aim of this part of our study was to adjust the functional empirically with a time-efficient method.

Calculations with the aim to probe the effect of changes of the nuclear charge of the copper center on the spin density distribution were done with ORCA, using the BLYP functional together with Ahlrichs triple ζ basis set[45] with an additional polarization function on Cu, a triple ζ basis set on N, Cl, C, and O, and a double ζ basis set with additional polarization on H.[45,46] (The ORCA basis set "CoreProp" was used on Cu. This is based on the TurboMole DZ basis developed by Ahlrichs and coworkers and obtained from the basis set library under ftp.chemie.uni-karlsruhe.de/pub/basen.)

The Energy decomposition analysis[47–50] was performed with the BP86 functional and a triple ζ basis set, using ADF.

Calculation of Spectroscopic Parameters

For studies on spectroscopic parameters the B3LYP/6-31G(d)-optimized structures were used for density functional theory calculations, using the ORCA suite of programs to calculate the **g**, **A**, and **a** tensors of $[Cu(L^{1b})(Cl)]^+$. For these calculations Ahlrichs triple ζ basis set with an additional polarization function on Cu, a triple ζ basis set on N, Cl, C, and O and a double ζ basis set with additional polarization on H were used, unless specifically mentioned. To obtain a good estimate of the EPR parameters the flexible CP(PPP) basis set (the ORCA basis set "CoreProp" was used for Cu. EPR properties were predicted by coupled, perturbed Kohn–Sham theory for the g-tensor and the spin-orbit coupling contribution to the hyperfine coupling tensor.[51] Fermi contact terms and spin–dipole contributions were obtained as expectation values from the ground state spin density. Ligand field calculations based on density functional theory (LF-DFT)[41] were used to calculate the d–d transitions of $[Cu(L^{1b})(Cl)]^+$, and the results were compared with the SORCI[37] calculations and experimental data.

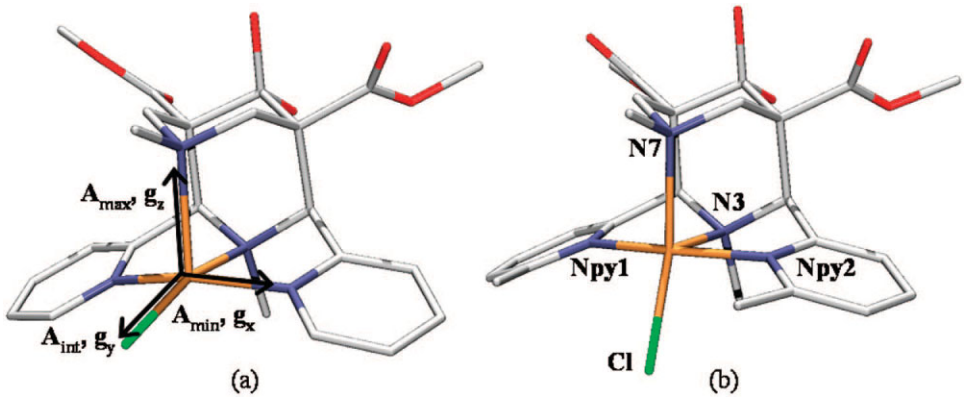

Figure 3. Plots of the molecular structures of (a) $[Cu(L^{1b})(Cl)]^+$ and (b) $[Cu(L^{2b})(Cl)]^+$, with the predicted orientation of the **g**-tensor, predicted by the B3LYP calculations of $[Cu(L^{1a})(Cl)]^+$.

Results and Discussion

Experimental Determination of the g-, A-, and a-Tensor Parameters and the Spin Distributions.

The frozen solution EPR spectrum of $[Cu(L^{1b})(Cl)]^+$ in DMF/MeOH at 116 K is shown in Figure 2. The spectrum shows the typical features of a Cu(II) center with a pseudoaxial symmetry and a $d_{x^2-y^2}$ ground state, that is, $g_\parallel > g_\perp > 2.00$, and with a large parallel hyperfine splitting parameter ($A_\parallel = 150$–$200\ 10^{-4}cm^{-1}$); see Figure 3 for the orientation of the **g** and **A** tensor axes. The perpendicular region of the hyperfine splitting is partially resolved and one of its feature overlaps with the parallel transitions. The super hyperfine transitions due to the four nitrogen donors (N3, N7, Npy1, Npy2) and the coligand Cl are also observed in the perpendicular region.

For the simulation of the spectrum, coupling of the electron spin with the nuclear spins of Cu (I = 3/2), N3, Npy1, Npy2 (I = 1) and Cl (I = 3/2) was considered. The Cu–N7 vector lies along the Jahn–Teller axis and therefore N7 is expected to have negligible contributions from the super hyperfine splitting pattern. Density functional theory calculations support this assumption. The spin Hamiltonian parameters obtained from the simulation of the experimental spectrum (see Fig. 2), together with those from the DFT calculations are shown in Table 1.

Based on ligand field theory,[16,52–56] the hyperfine parameters of a d^9 complex with tetragonal symmetry and the unpaired electron in the $d_{x^2-y^2}$ orbital are given as:

$$A_\parallel = P\left(\frac{-4\alpha^2}{7} - K\alpha^2 + \frac{3\delta g_\perp}{7} + \delta g_\parallel\right) \tag{3}$$

$$A_\perp = P\left(\frac{2\alpha^2}{7} - K\alpha^2 + \frac{11\delta g_\perp}{14}\right). \tag{4}$$

Here, $P = g_e g_N \beta_e \beta_n \langle r^{-3}\rangle$, which is generally assumed as $360 \cdot 10^{-4}$ cm^{-1},[57] K is the Fermi contact contribution, and α^2 is the relative amount of metal character in the ground state wave function and, therefore, represents the degree of covalency of the copper–ligand bonding. $\alpha^2 = 1$ indicates an ionic bond and $\alpha^2 = 0.5$ indicates a covalent bond. With the spin Hamiltonian parameters from the experimental spectrum (see Table 1) eqs. (3) and (4) yield $K = 0.27$, and $\alpha^2 = 0.87$, which is consistent with similar values reported for other Cu(II) complexes.[52]

From the super hyperfine coupling values it is possible to calculate the spin density present in the s and p orbitals of the ligand donor atoms. These can be calculated by eqn. (5) and (6).[55]

$$\rho_s = \frac{\left(\frac{a_x + a_y + a_z}{3}\right)}{a_{iso*}} \tag{5}$$

$$\rho_p = \frac{\left(\frac{a_\parallel - a_\perp}{3}\right)}{a_{aniso*}}. \tag{6}$$

Here, ρ_s and ρ_p are the spin densities on the s and p orbitals, respectively; a_{iso*} is the isotropic splitting observed due to an electron in an s orbital, and a_{aniso*} is the anisotropic splitting observed due to an electron in a p orbital of the free atom.[55] The spin densities on the s and p orbitals of the relevant donor atoms, based on the experimental spectrum and eqs. (5) and (6) are also given in Table 1. The sum over all calculated spin densities on s and p orbitals of the ligand is 21.7%, reasonably consistent with $\alpha^2 = 0.87$.

It is important to note here that eqs. (3)–(6) are based on ligand field theory, and also based on the assumption that the copper(II) ion has axial symmetry. Ligand field theory is a one-center approximation and the spin densities obtained from a Mulliken population analysis also contain overlap terms.[58] Also, in $[Cu(L^{1b})(Cl)]^+$, the symmetry of the chromophore is lower than D_{4h}. In C_s symmetry there is direct mixing of the σ and π-orbitals and, therefore, the obtained spin densities should be treated with

Table 1. Spin Hamiltonian Parameters of $[Cu(L^{1a})(Cl)]^+$ Obtained by Simulation of the Experimental Spectrum and DFT (B3LYP) Calculations.

Parameter	Simulations	B3LYP	Isotropic	Dipolar	Spin-orbit
$g_\perp$	2.050	2.058			
$g_\parallel$	2.224	2.162			
A_x	18.0	4.8	−88.6	68.8	24.8
A_y	22.0	22.0	−88.6	90.6	20.0
A_z	(−)175.0	−88.6	−174.6	−159.4	73.5
a_x^{N3}	8.0	7.8	9.7	−1.9	−0.1
a_y^{N3}	10.6	13.4	9.7	3.7	0
a_z^{N3}	8.0	7.8	9.7	−1.8	−0.05
a_x^{Npy}	14.0	15.5	13.1	2.3	0
a_y^{Npy}	12.0	11.7	13.1	−1.3	0
a_z^{Npy}	12.0	12.1	13.1	−1.0	−0.06
a_x^{Cl}	(−)7.4	−3.6	5.0	−8.0	−0.5
a_y^{Cl}	15.3	21.1	5.0	16.1	0.0
a_z^{Cl}	(−)7.4	−4.2	5.0	−8.0	−1.2
ρ_s; ρ_p(N3)	1.7; 2.7				
ρ_s; ρ_p(Npy)	2.5; 2.1				
ρ_s; ρ_p(Cl)	0.01; 8.1				
$K = 0.27$					
$\alpha^2 = 0.868$					

A and a values in 10^{-4} cm^{-1}.

caution.[54,58–60] Other possible sources of error for the spin densities calculated with eqs. (3) and (4) arise from the assumed value for P[54,57] and possible inaccuracies introduced by the spectra simulations. For all this reasons, the SORCI calculations are used as the reference for the computed spin densities. For $[Cu(L^{1b})(Cl)]^+$ the SORCI-derived spin density on Cu is 0.848. The "experimental," ligand–field-based value of 0.87 is in good agreement with this and also with other similar studies. This suggests that a realistic value for the spin density on Cu of $[Cu(L^{1b})(Cl)]^+$ is in the range of 0.85 to 0.87. This value is therefore taken as the reference for the various calibration procedures below.

Structures and Isomerism

Calculations have been performed on $[Cu(L^1)(Cl)]^+$ and $[Cu(L^2)(Cl)]^+$, both of which have been characterized experimentally by X-ray crystallography, spectroscopy, and thermodynamic properties.[27,29] The two experimental structures are drastically different (see Fig. 3), and this has been interpreted on the basis of a subtle balance between steric and electronic effects.[23,30] Other properties (redox potentials, stabilities, and reactivities) have been found to correlate with the structural differences.[26,27,32] DFT calculations indicate that the electronically favored coordination geometry of the bispidine ligand copper(II) complex is a square pyramidal structure with Cl coplanar with the two pyridine rings and *trans* to N3, and with an elongated axial Cu—N7 bond, similar to the experimentally observed structure (named here *trans N3*).[28] Substitution at the α-position of the pyridine rings with methyl groups leads to a trigonal–bipyramidal distortion of the optimized *trans N3* structure, and also gives rise to a second minimum, in which the coligand binds *trans* to N7 (the *trans N7* structure), with a relatively short Cu—N7 and slightly elongated Cu—N3 bond.

Experimentally, the *trans N3* isomer is the only observed structure of $[Cu(L^{1b})(Cl)]^+$,[23,28,29] which indicates that this geometry is enforced by the bispidine ligand. Indeed, other pentacoordinate complexes of L^1, such as Cu^I and Zn^{II} have the same geometry. With L^2, where coordination in the *trans N3* position is hampered by steric bulk, the only minimum found experimentally is the *trans N7* isomer. Although the calculations predict the existence of the *trans N7* isomer for $[Cu(L^2)(Cl)]^+$ with acceptable structural agreement with experiment, this isomer is calculated at the B3LYP/6-31G(d) level to be less stable than the trigonal–bipyramidally distorted *trans N3* isomer by 11 kJ/mol. With a triple-ζ basis set the energy difference is only slightly increased (12–13 kJ/mol). Exploration of the potential energy hypersurface along the N7–Cu–Cl angle from 90° to 180° did not yield a minimum for a *trans N7* isomer for L^1. This indicates that the *trans N7* isomer is electronically unfavorable, and can only be enforced by destabilization of the *trans N3* isomer, for example, by steric hindrance.

The above discussion pertains to the complexes in which there is a C═O group at C9 (L^{1a}, L^{2a}). For the purpose of computation this group is convenient due to the increased symmetry (C_S) of the complex. However, because both experimental structures discussed here have a hydrolyzed backbone, the differences between the computed structures of the complexes with the two different forms of the ligand were investigated. The main changes are found in the bond distances, variations in the angular geometry are negligible. In particular, the nonbonded N3 · · · N7 and Npy1 · · · Npy2 distances remain approximately constant. The general effect

Table 2. Energy Decomposition Analysis (EDA) of $[Cu(L)(Cl)]^+$ (L^{1a}, L^{2a}, *trans* N3, *trans* N7 Geometries, ΔE in kJ/mol).

		L	Cl+Cu+L	{CuCl}+L	{CuL}+Cl
trans N3-$[Cu(L^{2a})(Cl)]^+$	ΔE_{int}	−30618.4	−2586.4	−697.8	−1014.5
	ΔE_{Pauli}	118587.0	842.8	649.9	548.7
	ΔE_{elstat}	−24937.3(16.7%)	−2244.9(65.5%)	−723.5(53.7%)	−1014.9(64.9%)
	ΔE_{orb}	−124268.3(83.3%)	−1184.3(34.5%)	−624.2(46.3%)	−548.2(35.1%)
trans N7-$[Cu(L_{2a})(Cl)]^+$	ΔE_{int}	−30607.8	−2587.2	−703.4	−857.1
	ΔE_{Pauli}	118613.8	888.3	795.8	513.2
	ΔE_{elstat}	−24930.5(16.7%)	−2246.4(64.6%)	−814.6(54.3%)	−1001.3(73.1%)
	ΔE_{orb}	−124290.9(83.3%)	−1229.2(35.4%)	−684.7(45.7%)	−369.0(26.9%)
trans N3-$[Cu(L_{1a})(Cl)]^+$	ΔE_{int}	−27444.8	−2619.8	−732.2	−927.9
	ΔE_{Pauli}	107890.7	914.2	783.0	515.1
	ΔE_{elstat}	−22821.6(16.9%)	−2307.7(65.3%)	−823.5(54.3%)	−1034.3(71.7%)
	ΔE_{orb}	−112513.8(83.1%)	−1226.3(34.7%)	−691.7(45.7%)	−408.8(28.3%)
trans N7-$[Cu(L_{1a})(Cl)]^+$	ΔE_{int}	−27441.0	−2561.8	−674.2	−870.0
	ΔE_{Pauli}	108056.0	975.6	879.0	531.5
	ΔE_{elstat}	−22859.9(16.9%)	−2312.4(65.4%)	−866.8(55.8%)	−1003.5(71.6%)
	ΔE_{orb}	−112637.1(83.1%)	−1225.1(34.6%)	−686.4(44.2%)	−398.1(28.4%)

of the hydrolysis of the carbonyl group is, as expected,[22,27,61] to decrease the bond distances of the Cu to the donor atoms of the bispidine ligand. This effect is most pronounced for the Cu—N7 bond distances in the *trans N3* structures.

The relative energy between the two isomers of $[Cu(L^2)(Cl)]^+$ changes by less than 1 kJ/mol upon hydrolysis of the carbonyl group (L^{2a} vs. L^{2b}). Also, the spin density on the copper center is virtually unaffected by the hydrolysis, and the spin densities on the ligands are only slightly affected. In conclusion, therefore, the changes between the keto and the hydrolyzed forms of L^1 and L^2 in geometry and, more importantly, in electronic structure and relative energies, are negligible, making the ketone-based ligands valid models for the computational studies.

Energy Decomposition Analysis

An EDA[40,47–50,62] was used for the further analysis of the energy difference between the two isomers. The interaction energy between fragments (ΔE_{int}) is decomposed into three main components [eq. (7)].

$$\Delta E_{int} = \Delta E_{elstat} + \Delta E_{Pauli} + \Delta E_{orb} . \quad (7)$$

The ΔE_{elstat} term describes the electrostatic interaction between the fragments, ΔE_{Pauli} refers to the closed shell (Pauli) repulsive interaction, and ΔE_{orb} is the electronic stabilization term, calculated in the final step of the EDA analysis, when the Kohn–Sham orbitals relax to their final form.

The results of the EDA for $[Cu(L^{1a})(Cl)]^+$ and $[Cu(L^{2a})(Cl)]^+$ are summarized in Table 2. The total attractive interaction is due to ΔE_{elstat} and ΔE_{orb}, and the percentage contribution of each of these terms to the total attractive interaction is given in parentheses. The calculations using atomic fragments of $[Cu(L^{2a})(Cl)]^+$ stabilize the *trans N3* geometry over the *trans N7* isomer by 9.8 kJ/mol, which is consistent with the Gaussian calculations above (12–13 kJ/mol) but inconsistent with experiment.

For $[Cu(L^{2a})(Cl)]^+$, single-point energies of the ligand fragments L, fixed in their *trans N3* and *trans N7* geometries, indicate that the ligand in the *trans N3* isomer has an energy which is 10.6 kJ/mol lower than in the *trans N7* isomer. The components of ΔE_{int} reveal that, while the repulsive Pauli interaction and the stabilizing electrostatic interaction destabilize *trans N7* relative to *trans N3* by approximately 34 kJ/mol, this is partly compensated by the stabilizing orbital interaction, which favors *trans N7* by approximately 23 kJ/mol. Qualitatively, this is in agreement with molecular mechanics calculations (single-point calculations of the ligand portions, based on the X-ray and DFT-optimized structures, using the MOMEC program and force field).[63,64] However, the MM-based destabilization of the *trans N7* isomer of approx. 3 to 6 kJ/mol, is much smaller. EDA calculations with Cl, Cu, and L treated as a separate fragments (Cl+ Cu+ L), and CuCl and L treated as separate fragments ({CuCl}+ L) stabilize the *trans N7* isomer by 0.8 kJ/mol and 5.6 kJ/mol, respectively. Here, the Pauli interactions favor *trans N3*, and the stabilizing electrostatic and orbital interactions favor *trans N7*. In both cases the attractive interactions dominate the repulsive term, resulting in a stabilization of *trans N7* over *trans N3* (see Table 2). A further calculation, performed with separate CuL and Cl fragments ({CuL}+ Cl) results in a stabilization of the *trans N3* isomer by 157.4 kJ/mol. Here, the total attractive interactions, due to ΔE_{elstat} and ΔE_{orb}, are significantly different for the two isomers. The artificial stabilization of the *trans N3* isomer, compared to experiment, is primarily due to the preference of the ligand for the *trans N3* coordination geometry, and a large stabilizing orbital interaction energy for the *trans N3* isomer from the {CuL}+Cl fragment interaction.

Table 3. The Influence of the Functional on the Spin Density Distribution in $[Cu(L^{1a})(Cl)]^+$ and $[Cu(L^{1b})(Cl)]^+$ (*trans* N3 Isomer).

Atom	BLYP	BP86	B3LYP	B3P86	PBE	B(38HF) LYP	B(38HF) P86	BHandH LYP	B(61HF) LYP	B(61HF) P86	SORCI[a]	exp
$[Cu(L^{1a})(Cl)]^+$												
Cu	0.575	0.569	0.672	0.665	0.700	0.771	0.758	0.812	0.864	0.840	—	—
N7	0.001	0.002	0.000	0.000	0.000	−0.001	−0.001	0.001	−0.001	−0.001	—	—
N3	0.104	0.107	0.082	0.084	0.076	0.059	0.063	0.050	0.037	0.044	—	—
Npy1,2	0.072	0.072	0.063	0.064	0.060	0.049	0.052	0.044	0.035	0.040	—	—
Cl	0.154	0.152	0.114	0.115	0.101	0.077	0.080	0.061	0.044	0.051	—	—
$[Cu(L^{1b})(Cl)]^+$												
Cu	0.575	0.569	0.673	0.665	0.701	0.772	0.758	0.813	0.865	0.840	0.848	0.868
N7	0.002	0.003	0.000	0.000	0.000	−0.001	−0.001	0.001	−0.001	−0.001	0.000	0.000
N3	0.110	0.114	0.085	0.088	0.080	0.061	0.066	0.052	0.038	0.045	0.036	0.044
Npy1,2	0.071	0.071	0.063	0.064	0.060	0.049	0.052	0.044	0.035	0.040	0.027	0.046
Cl	0.150	0.149	0.111	0.112	0.099	0.075	0.078	0.060	0.042	0.050	0.050	0.082

[a]See text for the computational details.

This relates to one of the most intriguing and for copper(II) (probably in general for transition metal) bispidine coordination chemistry most important observations: the orbital interaction strongly favors coordination of Cl^- to the $\{CuL\}^{2+}$ fragment *trans* to N3 (that is the *trans N3* vs. the *trans N7* geometry). This also follows from the spectroscopic analysis (see below), which indicates that this is due to a subtle balance of the π acceptor properties of the pyridine and the π donor properties of the coligand (Cl^- in the present case), and it is in agreement with the experimentally determined $[Cu(L)(OH_2)]^{2+}$ formation constants.

For $[Cu(L^{1a})(Cl)]^+$, a *trans N7* isomer has not been located. Therefore, the optimized *trans N3* isomer structure with a constrained N7–Cu–Cl angle of 165° (as is found in the *trans N7* structure of $[CuL^2Cl]^+$) was used for the analysis. In summary, all fragment type calculation show that the *trans N3* isomer is more stable than *trans N7* isomer, in agreement with experiment. The percentage of the attractive interaction remains constant for both isomers in all calculations. For all fragment type calculations ΔE_{int} of the *trans N3* isomer is approx. 60 kJ/mol lower in energy than that of *trans N7*.

The Role of the Functional on the Spin Density Distribution

In analogy to the calculations performed for $[Cu(Cl)_4]^{2-}$,[7] a set of DFT calculations with varying amounts of HF exchange were done for $[Cu(L^{1a})(Cl)]^+$, $[Cu(L^{1b})(Cl)]^+$, and $[Cu(L^{2a})(Cl)]^+$, using the 6-31G(d) basis set and a range of functionals implemented in Gaussian 03. For L^{1a} and L^{1b} five pure DFT functionals (0% HF exchange), three B3X-type functionals (Becke's three-parameter hybrid exchange functional with different correlation functionals, 20% HF exchange), the PBE[65,66] (25% HF exchange) and BHandHLYP[14] functionals (50% HF exchange) were tested. For L^{2a} only five of the above functionals were used, as it was shown for L^1 that the spin density is relatively unaffected by different correlation functionals. For comparative purposes, spin densities at the *ab initio* HF level were also calculated for both complexes. Results for selected functionals are summarized in Table 3 for L^{1a} and L^{1b}, the results for L^{2a} are given as supplementary material; Table 3 also includes the SORCI and "experimental" spin density data for comparison.

The main delocalization of the single unpaired d-electron from the copper center in $[Cu(L^{1a})(Cl)]^+$ is to Cl and the tertiary amine donor N3, slightly less spin density is donated to the two pyridine donors, and the spin density on N7 is negligible (see also Fig. 4). This is in agreement with the model used for the calculation of the hyperfine splitting in the EPR spectrum, where only N3, Npy, and Cl were considered to contribute to the spin density delocalization. Hydrolysis of the carbonyl group at C9 to a diol has a negligible effect on the spin density of the copper center.

A linear dependence of the spin density on the copper center from the amount of HF exchange in the hybrid functional is observed, which turns out to be independent of the nature of the correlation functional. For $[Cu(L^{1a})(Cl)]^+$ the spin on copper varies between ~0.57 for the pure DFT functionals (0% HF), ~0.672 for the Becke three-parameter hybrid functionals and 0.812 for the BHandH (50% HF) functional. The spin density on the copper center calculated with *ab initio* HF theory is 0.931. The spin on the Cl, N3, and Npy donors decreases as the spin on the copper center increases and these relationships are also linear. This is shown graphically for $[Cu(L^{1a})(Cl)]^+$ in Figure 5. For $[Cu(L^{2a})(Cl)]^+$, both in the *trans N3* and in the *trans N7* isomers, a similar linear relationship is observed (see supplemental material).

From the linear dependence of the copper spin density (see eqs. in Fig. 5) on the amount of HF exchange and the known value of 0.87 in $[Cu(L^1)(Cl)]^+$ (SORCI and "experiment"), the amount of HF exchange required to reproduce the reference spin density is calculated to 61%, considerably higher than the 38% found to be optimal for $[Cu(Cl)_4]^{2-}$.[7] Calculations with an adjusted BLYP functional, incorporating 61% HF exchange (denoted B(61HF)LYP), were performed and the result of 0.865 for the spin density of Cu is in good agreement with the reference value (see

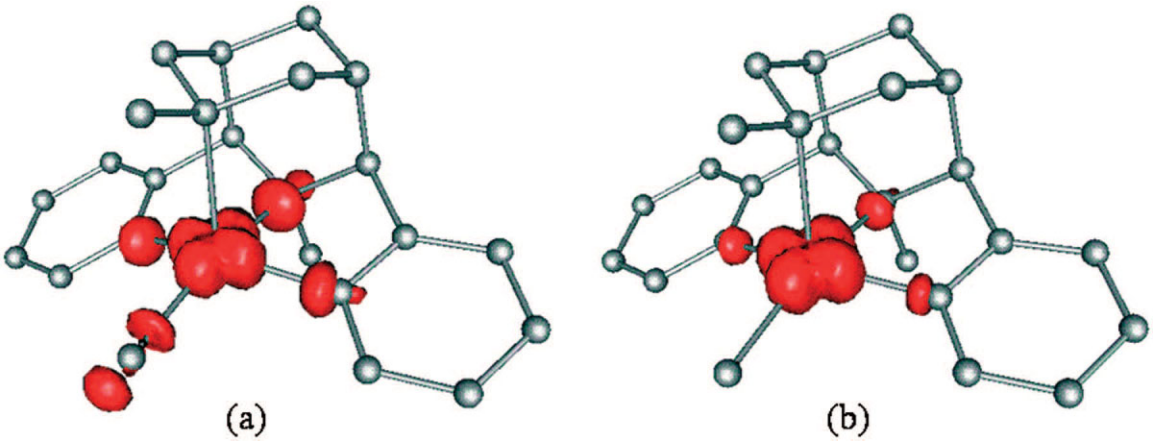

Figure 4. Spin densities of $[Cu(L^{1a})(Cl)]^+$, calculated with the BLYP (a) and B(61HF)LYP (b) functionals.

Table 3). With an adjusted B(61HF)P86 functional, the calculated spin density is slightly lower (0.840), but still in good agreement with the reference value. For comparison, the B(38HF)LYP and B(38HF)P86 functionals give spin densities of 0.771 and 0.758, significantly lower than the reference value.

Although the B(61HF)LYP functional improves the calculated spin on copper, a spin of around half of the "experimental" value for Cl and slightly lower than "experiment" for N3 and Npy are predicted (note, however, the small values resulting in a relatively large error limit). The comparison with the SORCI reference value gives better agreement, both with B(61HF)LYP and B(61HF)P86. The spin densities on the ligands also have a linear dependence on the amount of HF exchange, and from these graphs an optimal amount of HF exchange, necessary to reproduce the "experimental" spin densities or the reference value (SORCI) can be determined for each of the ligands, analogous to the method used for copper. Although the spin density on copper is not dependent on whether a diol or a carbonyl group is substituted at C9, the spin densities on the ligands are to some extent. Interestingly, the required amount of HF exchange for Cl, based on the "experimental" value, is close to the 38% determined to be optimal for $[CuCl_4]^{2-}$. As expected,[7] of all the functionals tested, the B(38HF)LYP functional gives the best agreement with the "experimental" value for Cl (see Table 3). Based on the SORCI reference value, both B(61HF)X (X=LYP, P86) functionals are to be preferred. This indicates that there is no general optimum functional for all complexes of a given metal ion. However, the contribution to the total spin density from the ligands is much smaller than the contribution of the metal center. Therefore, an improvement of the electronic description of the metal at the expense of the ligands still may give a better description of the electronic structure of the complex as a whole. As N3 and Npy contribute only slightly to the total spin density and are less dependent on the amount of HF exchange in the functional, the main task was therefore to balance the functional for Cu and Cl.

Modification of the Nuclear Charge of Copper to Adjust the Spin Density Distribution

An alternative approach to adjust the spin density distribution is to modify the nuclear charge of the copper center ($Q = 29$). Previously, the use of a pure functional with the nuclear charge of $Q = 28.2$ on the copper center has been suggested to obtain good estimates of the spin densities, based on studies of the $[Cu(dien)_2]^{2+}$ complex (dien = 3-azapentane-1,5-diamine).[18] A range of DFT calculations with $[Cu(L^{1+})(Cl)]^+$, in which the nuclear charge of the Cu atom was systematically varied from 29 to 28 with a step of 0.2, were performed with ORCA and the BLYP functional. The resulting spin densities are listed in Table 4. The spin density on the metal center increases with decreasing nuclear charge. Good agreement of the spin densities on the metal and the ligands is obtained with BLYP and $Q = 28.2$. The calculations were also performed with a hybrid B3LYP functional, and these results are given as supplementary material. (Note that the hybrid functional are already optimized against the experimental results and modifying the nuclear charge on hybrid functional will question the reliability of the approach.)

The Influence of the Functional on the Geometries and Relative Energies of $[Cu(L^1)(Cl)]^+$ and $[Cu(L^2)(Cl)]^+$

A comparison of the calculated structures of $[Cu(L^{1b})(Cl)]^+$ with the different functionals is given in Table 5. On the whole, the hybrid functionals perform better for angles, but slightly overestimate the bond distances, and this overestimation increases as more HF exchange is added. The nonhybrid functionals generally give a better description of the bond lengths but worsen the angular geometry. So, although the spin densities are improved by increasing HF exchange, this is done at the expense of the geometries.

The geometries and relative energies of the two isomers of $[Cu(L^{2b})(Cl)]^+$ were compared with a range of functionals, in an attempt to find a solution to, or at least an explanation for, the problem of the computed destabilization of the experimentally observed *trans N7* structure, relative to the *trans N3* isomer. The results are summarized in Table 6. Although the energy difference between the two isomers is decreased with two of the functionals relative to the B3LYP value none of the functionals predict the *trans N7* isomer to be more stable.

Although the calculated geometries of the *trans N7* isomer of $[Cu(L^{2b})(Cl)]^+$ show an overall acceptable agreement with exper-

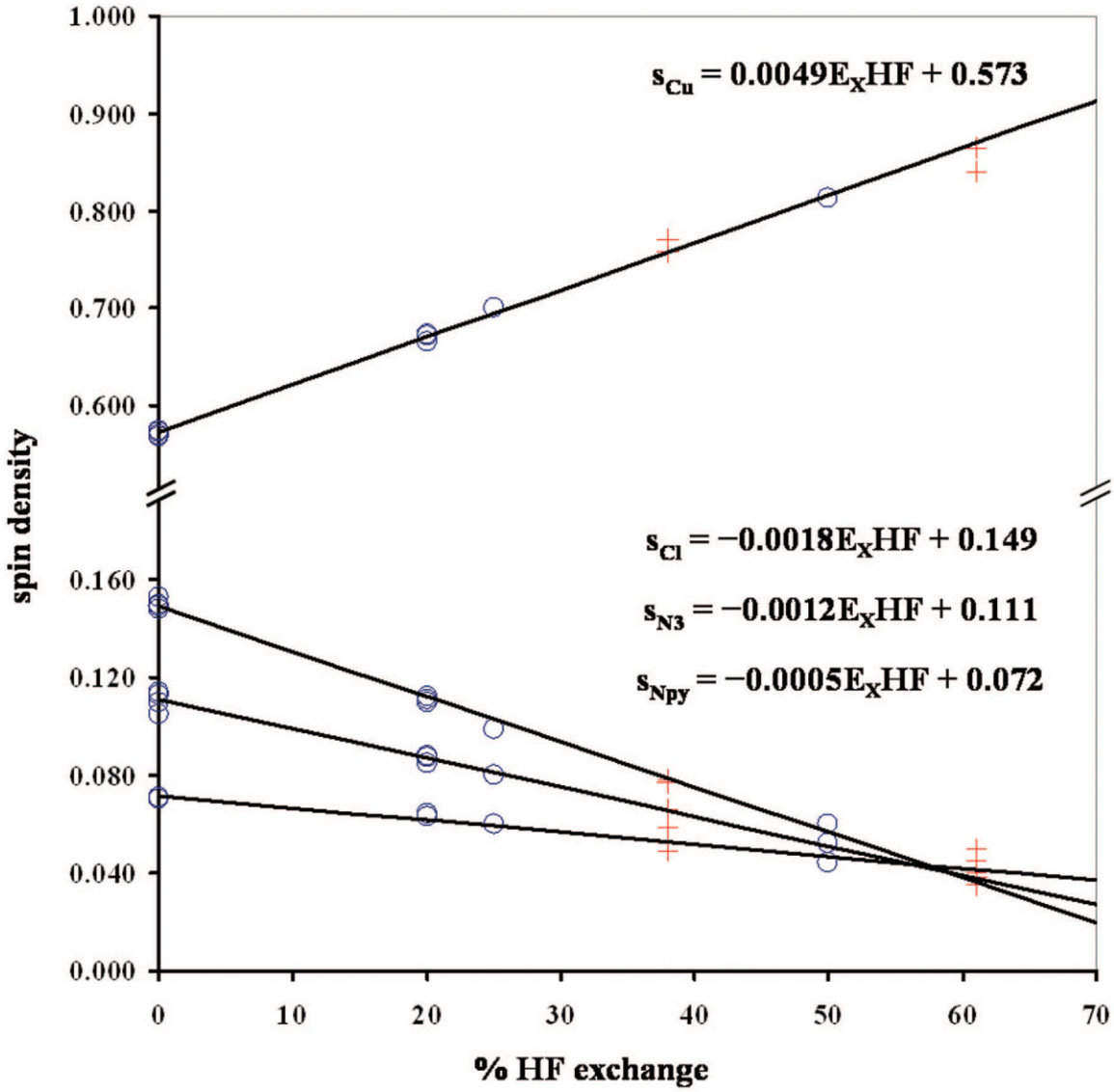

Figure 5. Plots of spin density vs. % HF exchange for (left, from top to bottom) Cu, Cl, N3, and Npy in $[Cu(L^{1a})(Cl)]^+$, ○: Gaussian 03 implemented functionals (used for straight line fitting), +: modified functionals.

iment for all functionals, the computed Cu—N3 bonds are consistently shorter than the Cu—N7 bonds. This is in contrast to the crystal structure, where the Cu—N3 bond is, as expected, slightly longer than the Cu—N7 bond (0.03 Å). Interesting to note is that the two functionals that give the smallest error in relative energy (PBE, B3P86) also have the smallest Cu—N7/Cu—N3 ratio. For the PBE and B3P86 functionals this ratio is 1.01 and the relative energies are 5.6 and 6.2 kJ/mol, respectively. For B3LYP and BHandH the ratios are larger (1.02 and 1.03, respectively) and the relative energies increase to 9.2 and 9.9 kJ/mol, respectively. The energy difference obtained with the HF/6-31G(d) method gives a Cu—N7/Cu—N3 ratio of 1.08 and an energy difference of 12.5 kJ/mol, significantly worse than with any of the DFT functionals. Incorrect prediction of the relative bond distances to N7 and N3 could lead to a loss of electronic stabilization (pseudo Jahn–Teller effect) in the calculated *trans* N7 structures, and may well be the reason for the destabilization of the experimentally observed *trans* N7 isomer of $[Cu(L^{2a})(Cl)]^+$ and $[Cu(L^{2b})(Cl)]^+$.

There is no direct correlation between the description of the bonding (amount of HF exchange), the relative energy of the two isomers and the Cu—N7/Cu—N3 ratio. The choice of the best functional for the calculation of copper–bispidine complexes does not appear to be as simple as for $[Cu(Cl)_4]^{2-}$, where the covalence of the bonds is the only significant factor in determining the bond lengths and energies. While the correlation functional does not influence significantly the spin density distribution, it does have a significant influence on the geometries and relative energies. The P86 correlation functional predicts shorter bond lengths than LYP,

Table 4. The Influence of the Nuclear Charge of the Cu Center on the Spin Density Distribution in $[Cu(L^{1a})(Cl)]^+$.[a]

Atom	BLYP (Q = 29)	BLYP (Q = 28.8)	BLYP (Q = 28.6)	BLYP (Q = 28.4)	BLYP (Q = 28.2)	BLYP (Q = 28.0)	SORCI[b]	Exp.[b]
Cu	0.507	0.599	0.680	0.763	0.871	1.034	0.848	0.868
N7	0.001	0.000	0.000	0.002	0.007	0.015	0.000	0.000
N3	0.127	0.106	0.089	0.078	0.070	0.064	0.036	0.044
Npy1	0.088	0.074	0.061	0.048	0.031	0.006	0.027	0.000
Npy2	0.088	0.074	0.061	0.048	0.031	0.007	0.027	0.046
Cl	0.179	0.146	0.119	0.100	0.086	0.076	0.050	0.082

[a]BLYP, ORCA.
[b]L^{1b}.

in better agreement with the experiment. Changing from the B3LYP to the B3P86 functional reduces both the Cu—N7 and the Cu—N3 bond lengths, but has a larger effect on Cu—N7 than on Cu—N3. Consequently, ΔE between the two isomers is decreased by 3 kJ/mol. The change in ΔE upon a further change from B3P86 to B(61HF)P86 (an increase in HF exchange of 41%) is negligible.

The calculations described so far have all been done in the gas phase, and the possibility that environmental effects might stabilize the *trans N7* isomer have been probed by solution phase geometry optimization of both isomers of $[Cu(L^{2a})(Cl)]^+$, using the PCM model as implemented in Gaussian03 with acetonitrile as the solvent. Indeed, this has the effect of decreasing ΔE to 4 kJ/mol (from 9 kJ/mol in the gas phase) for B3LYP/6-31G(d), although the *trans N3* isomer remains more stable. For the B3P86 functional, the energy is almost degenerate (ΔE between the isomers less than 1 kJ/mol). Because we have shown that ΔE is relatively insensitive to the amount of HF exchange, for the P86 correlation functional, we expect that the addition of solvation to the B(61HF)P86 functional will also give close to degenerate structures.

The *trans N3* and *trans N7* geometries of $[Cu(L^{2a})(Cl)]^+$, optimized at B3LYP/6-31G(d), have also been used to calculate the energy with the SORCI method. For these calculations, the Ahlrichs triple ζ basis set for the metal center and a double ζ basis set for the nonmetal atoms have been employed. Without solvation, the SORCI calculation predicts the *trans N3* isomer to be more stable than the *trans N7* isomer by 13.6 kJ/mol (consistent with the Gaussian03 and ADF predictions). However, using the COSMO solvation model implemented in ORCA and acetronitrile as the solvent, the reverse order is obtained, that is, the *trans N7* isomer is more stable by 7.9 kJ/mol than the *trans N3* geometry. This demonstrates that solvation effects are important and can significantly influence the results, especially when the energy differences are small.

The Calculation of Spectroscopic Parameters

For the calculation of the EPR parameters of $[Cu(L^{1a})(Cl)]^+$ a reasonably accurate prediction was obtained with the B3LYP functional (see Table 1). The calculated orientation of the g-tensor axis is shown in Figure 3. The calculated $g_\perp$ values are in good agreement with the experiment, but the calculated, $g_\parallel$ is lower than observed. This has been previously found for other Cu(II) complexes using the B3LYP functional and a better agreement has been obtained using SORCI calculations.[67]

The computed hyperfine splittings follow the experimentally observed order $A_x < A_y < A_z$. The calculated A_x values are too low but the A_y and A_z values are in good agreement with experiment. The largest component of the hyperfine splitting lies along the Cu—N7 axis, while the intermediate value is along Cu—Cl and

Table 5. Influence of the Functional on the Geometry of $[Cu(L^{1b})(Cl)]^+$.

Parameter	BLYP	BP86	B3LYP	B3P86	PBE	B(38HF) LYP	B(38HF) P86	BHandH LYP	B(61HF) LYP	B(61HF) P86	exp
Cu–N7	2.338	2.262	2.334	2.274	2.277	2.358	2.262	2.305	2.370	2.239	2.273
Cu–N3	2.069	2.044	2.058	2.035	2.037	2.077	2.040	2.068	2.106	2.047	2.042
Cu–Npy1/Npy2	2.020	1.997	2.028	2.005	2.011	2.056	2.017	2.043	2.090	2.022	2.022
Cu–Cl	2.271	2.249	2.239	2.219	2.218	2.240	2.213	2.228	2.249	2.208	2.232
N7–Cu–N3	86.82	87.89	85.80	86.48	86.14	84.82	86.04	85.15	84.02	85.60	85.03
N7–Cu–Cl	106.59	106.10	107.87	107.49	107.91	109.27	108.46	109.35	110.77	109.35	109.95
N3–Cu–Cl	166.59	166.01	166.33	166.03	165.96	165.91	165.50	165.50	165.21	165.04	165.02
Npy1–Cu–Npy2	154.19	153.30	155.49	155.21	155.35	155.44	155.31	155.19	154.36	155.10	158.13
Cu–N7/Cu–N3	1.130	1.106	1.134	1.117	1.118	1.135	1.109	1.115	1.125	1.094	1.113

Table 6. The Influence of the Functional on the Relative Energies and Geometries of the Two Isomers of $[Cu(L^{2a})(Cl)]^+$.

	trans N3, *trans* N7								
	BP86	B3P86	B3LYP	PBE	B(38HF)P86	BHandH	B(61HF)P86	HF	exp
Cu–N7	2.344, 2173	2.311, 2.157	2.374, 2.210	2.307, 2.164	2.282, 2.162	2.316, 2.219	2.251, 2.163	2.322, 2.332	2.120
Cu–N3	2.013, 2143	2.003, 2.141	2.023, 2.164	2.005, 2.140	2.006, 2.134	2.030, 2.147	2.011, 2.120	2.079, 2.150	2.147
Cu–Npy1/Npy2	2.080, 2.015	2.104, 2.028	2.132, 2.055	2.114, 2.036	2.129, 2.044	2.17, 2.079	2.143, 2.056	2.276, 2.171	2.063
Cu–Cl	2.231, 2.272	2.201, 2.237	2.220, 2.258	2.201, 2.234	2.195, 2.227	2.208, 2.240	2.191, 2.218	2.239, 2.263	2.221
N7–Cu–N3	87.29, 87.87	86.85, 87.12	86.20, 86.65	86.64, 86.75	86.61, 86.52	85.93, 85.61	86.22, 85.90	85.27, 83.58	86.71
N7–Cu–Cl	91.53, 162.94	93.49, 162.59	93.38, 162.20	93.96, 162.40	95.02, 161.45	95.99, 159.79	96.36, 160.13	99.35, 153.42	160.31
N3–Cu–Cl	178.82, 109.19	179.66, 110.29	179.58, 111.15	179.41, 110.86	178.37, 112.03	178.08, 114.60	177.42, 113.97	175.37, 123.00	112.97
Npy1–Cu–Npy2	144.58, 166.72	144.76, 165.33	145.2, 165.09	144.66, 164.92	144.62, 164.44	144.67, 163.56	144.54, 163.46	143.54, 160.65	163.83
Cu–N7/Cu–N3	1.164, 1.014	1.154, 1.007	1.174, 1.021	1.151, 1.011	1.138, 1.013	1.141, 1.034	1.119, 1.020	1.117, 1.085	0.987
ΔE (kJ/mol)	7.12	6.17	9.15	5.59	6.50	9.87	6.59	12.45	< -10

$\Delta E = E_{trans}(N7) - E_{trans}(N3)$

the smallest component along the two Cu—Npy bonds (see Fig. 3). The large value of A_z is mainly due to the dipolar term (−159.4), which is negative, while for A_x and A_y positive dipolar terms are obtained (68.8 and 90.6, respectively). This results in negative computed values for A_z and positive values for A_x and A_y (the simulated spectrum is insensitive to the sign of these parameters, see Table 1). The super hyperfine values calculated for N7 ($a_x = 0.14 \times 10^{-4}$ cm^{-1}, $a_y = 0.15 \times 10^{-4}$ cm^{-1}, $a_z = 0.18 \times 10^{-4}$ cm^{-1}) are very small and validate the model for the spectra simulation (see above). The principle components of the super hyperfine splitting for N3, Npy, and Cl are along the Cu—N3, Cu—Npy, and Cu—Cl bonds, respectively. The calculated values are in reasonable agreement with the experiment. The spin-orbit contribution to the metal hyperfine interactions are significant,[58] for Cl it is small and for N it is close to zero.

Although the B3LYP functional predicts the hyperfine and super hyperfine values reasonably well, the g values are too low. Therefore, we have attempted to calibrate the functional, based on the experimental g values. The amount of HF exchange was varied and additional calculations were performed with BLYP, B(38HF)LYP, and B(61HF)LYP (see Table 7). The pure BLYP functional underestimates both $g_{\perp}$ and $g_{\|}$, while the B(61HF)LYP functional overestimate them. The B(38HF)LYP functional provides acceptable estimates for both g-values.

It was of interest to test the computed g values with the approach of modifying the nuclear charge of the copper(II) center to $Q = 28.2$ (see above). With a pure BLYP functional and $Q = 28.2$ the $g_{\|}$ is underestimated and the $g_{\perp}$ values are overestimated (see Table 7). Based on the calculated spin densities with this setup (see Table 4), and based on the observation with the correlation of spin densities, bonding and spectroscopy above, this is not unexpected.

In the aqueous solution absorption spectrum of $[Cu(L^{1a})(Cl)]^+$ two broad bands are observed, one centered around 650 nm, the other around 900 nm. The electronic transitions of $[Cu(L^{1a})(Cl)]^+$ were calculated by SORCI and by LF-DFT. In the SORCI calculations, a reference space of CAS (9/5) was used to compute the ligand field transitions; the values of parameters to control the configurations that contribute to a particular state were as in the literature.[67] This predicted the transitions at 723, 729, 830 and 951 nm.

Considerable insight into the electronic structure of the $[Cu(L)Cl)]^+$ complexes can be gained by an analysis based on ligand field theory with parameters adjusted to DFT calculations. In the ligand field density functional theory (LF-DFT)[41] one assumes that transition metal d-orbitals in the complex are well defined and can be identified by the dominant contribution from the metal 3d functions. With complexes of Cu^{2+}, for example, a DFT calculation with an even occupation (9/5) of each d-orbital (average-of-configuration) is carried out. From the resulting Kohn–Sham eigenvalues and eigenvectors the one electron 5×5 matrix is computed. Complexes of Cu^{2+} are characterized by a single hole in the d^n subshell, which allows to discard effects of interelectronic repulsion. Furthermore, the spin-orbit coupling constant of Cu^{2+} in the complex can be obtained from its value for the free ion, weighted by an appropriate reduction factor for the unpaired electron, which is responsible for covalency in the complex. The latter has been chosen based on the percentage of the antibonding d-orbitals, which carry the unpaired electron of Cu^{2+}.

Table 7. Experimental and Computed g-Values with DFT and LF-DFT.

Parameters	$Q = 29$	$Q = 28.8$	$Q = 28.6$	$Q = 28.4$	$Q = 28.2$	$Q = 28.0$
Experiment						
$g_\perp$	2.050					
$g_\parallel$	2.224					
BLYP						
$g_\perp$	2.038	2.046	2.055	2.067	2.091	2.130
$g_\parallel$	2.109	2.130	2.145	2.154	2.161	2.171
B3LYP						
$g_\perp$	2.054					
$g_\parallel$	2.162					
PBE0						
$g_\perp$	2.061					
$g_\parallel$	2.185					
B(38)LYP						
$g_\perp$	2.073					
$g_\parallel$	2.224					
B(61)LYP						
$g_\perp$	2.093					
$g_\parallel$	2.300					
LF-DFT-PW91						
$g_\perp$	2.035				2.050	
$g_\parallel$	2.172				2.206	

Single-point calculations were performed with the ADF package using the PW91 functional and a valence triple ζ basis set on the optimized B3LYP/6-31G(d) structure. The chosen coordinate system for the calculation is shown in Figure 3. Orbital levels, their occupancies and Cu(3d) percentages are shown in Figure 6. Approximate orbital energy equations are given by the angular overlap model (AOM).

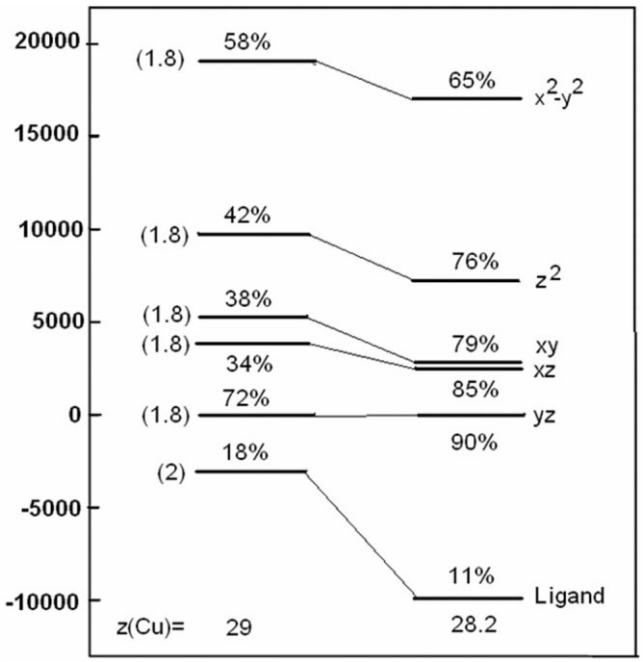

Figure 6. Energy level diagram with the sequence of the metal d and the ligand orbitals with their percent occupations.

$$E(d_{x2-y2}) = 3e_\sigma(\text{eq}) \tag{8}$$

$$E(d_{z2}) = e_\sigma(\text{eq}) + \text{e}_\sigma(\text{ax}) \tag{9}$$

$$E(d_{xy},d_{yz}) = e_\pi(\text{Cl}) \tag{10}$$

$$E(d_{xz}) = 2e_\pi(Npy)\ . \tag{11}$$

In eqs. (8)–(11) e_σ(eq) is the σ-bonding energy due to the ligands in the equatorial plane, due to the amine [N3, $e_\sigma(\text{N}_{\text{amine}})$], pyridine [Npy1 and Npy2, $e_\sigma(\text{N}_{\text{pyridine}})$], and Cl [$e_\sigma$(Cl)] donors; see eq. (12).

$$e_\sigma(\text{eq}) = \frac{3}{2}e_\sigma(N_{\text{pyridine}}) + \frac{3}{4}e_\sigma(N_{\text{amine}}) + \frac{3}{4}e_\sigma(\text{Cl})\ . \tag{12}$$

The parameter e_σ(ax) is the corresponding antibonding energy due to the axial ligand (N7), which accounts for the mixing of the 4s orbital with the 3d orbitals of the same symmetry (d_{z2}). Note, that the amine N donors N7 and N3 do not have orbitals for π-bonding. This is also the case for Npy in the pyridine plane, that is, d_{xy}, d_{yz}, and d_{xz} are only affected by π-orbitals of Cl and pyridine. The Kohn–Sham orbital energy diagram (Fig. 6, left) is in agreement with this simple description. The energies of the electronic transitions are listed in Table 8. These are overestimated in comparison to the experimental results. The PW91 functional exaggerates the metal–ligand covalency (see above), and this is manifested by the metal and Cl orbitals, which are close in energy and intermix

Table 8. Cu(3d) Orbital Energies (cm^{-1}) and Eigenvectors Projected from DFT Calculations (Ligand Field and Spin-Orbit Coupling Parameter and Energies of Electronic Transitions for $[Cu(L^{1b})C1]^+$.

Q(Cu) = 29 (PW91)					
Kohn–Sham eigenvalues:					
	19090	15243	13799	9315	0
Eigenvectors:					
xy	0.213	0.004	−0.613	0.001	0
yz	−0.818	0.003	−0.057	−0.001	−0.001
z^2	−0.012	−0.094	0.002	0.636	0.034
xz	0.007	0.562	0.005	0.117	−0.159
x^2-y^2	−0.001	−0.142	−0.001	0.053	−0.744
Ligand field matrix:					
	xy	yz	z2	xz	x^2-y^2
xy	13981				
yz	−964	18907			
z^2	−29	81	9407		
xz	12	−22	−748	14358	
x^2-y^2	−4	−29	942	−3238	794
Spin-orbit coupling constant: ζ = 512					
Orbital reduction factor: k=0.579					
Energies of d–d transitions:					
x2-y2→z2	1076 nm				
x2-y2→xy	724				
x2-y2→xz	653				
x2-y2→yz	521				

Q(Cu) = 28.2 (PW91)					
Kohn–Sham eigenvalues:					
	17065	14525	14194	9799	0
Eigenvectors:					
xy	−0.127	−0.018	0.877	0.000	0.000
yz	0.938	−0.004	0.137	0.001	−0.002
z^2	0.001	0.234	0.004	−0.839	0.109
xz	−0.001	−0.863	−0.018	−0.243	−0.210
x^2-y^2	−0.001	0.223	0.004	−0.002	−0.768
Ligand field matrix:					
	xy	yz	z2	xz	x^2-y^2
xy	14254				
yz	−410	17006			
z^2	−4	11	10008		
xz	6	−7	−897	13284	
x^2-y^2	−3	−28	1282	−3483	1023
Spin-orbit coupling constant: ζ = 571					
Orbital reduction factor: k=0.646					
Energies of d–d transition:					
			SORCI	exp.	
x2-y2→z2		1026	951	900 nm	
x2-y2→xy		709	830	650	
x2-y2→xz		680	729	650	
x2-y2→yz		581	723	650	

strongly. This decreases the metal percentage of the orbitals involved in the Cu—Cl π-overlap for d_{xy} and d_{xz} (see Fig. 6). Modified nuclear charge calculations with $Q = 28.2$ on copper and a pure functional (PW91) were therefore performed to overcome this problem. This results in an increased splitting of the close lying 3d and ligand orbitals and, therefore, reduces the artificial metal–ligand mixing. The accuracy of the calculated electronic transitions is improved and in acceptable agreement with the experimental values, specifically also in comparison with that of the SORCI calculation (see Table 8). Note, however, that the results of the SORCI calculations may be improved with a larger reference space.[67]

The computation of the **g** tensor components with the LF-DFT approach is described elsewhere.[68] The g-values obtained are shown in Table 7. These are underestimated with the PW91 functional, but with a Q value of 28.2 there is good agreement between the calculated and experimental g_z values. An acceptable agreement is also found for the $g_\perp$ values but there is a large anisotropy in the equatorial plane (LF-DFT-PW91, $g_{x,y} = 2.05$; $Q = 28.2$; $\Delta g_{x,y} = 0.07$). Probably, this anisotropy arises from a metal–ligand π-overlap, which is stronger for Cu—Cl than for Cu—Npy. LF-DFT calculations on $[CuCl_4]^{2-}$, $[Cu(NH_3)_4]^{2+}$, and *trans*-$[Cu(NH_3)_2(pyridine)_2]^{2+}$ model complexes allow to deduce values for e_π(Cl) and e_π(Npy) of 1950 and −450 cm^{-1}, respectively. These indicate that there is a strong donor function for Cl and a weak acceptor function for the pyridine donor. Considerable differences between the π-bonding properties of pyridine and Cl with Cu^{2+} imply a synergetic π-bonding, which might be responsible for the preference of these two ligands to coordinate the metal in a common plane. This readily explains the preference of Cl (or other π-donors) to coordinate in the basal rather then in an apical position with respect to the CuL fragments (see section on the isomer stabilities above). This is an important feature with respect to the specific reactivities and stabilities of copper(II) and other metal complexes with bispidine ligands, and this will now be studied in detail.

Conclusions

The generally available and commonly used DFT methods do not lead to an accurate description of copper(II)–donor interactions. HF calculations, DFT methods with pure DFT functionals, commonly used hybrid functionals and tuned functionals with varying amounts of HF exchange and various correlation functionals, have been used to optimize the DFT method, and the variation of the nuclear charge on copper together with a pure DFT functional has also been used to optimize the copper(II)–donor bonding description. Experimentally determined and computed (SORCI) spin distributions, experimental structures, isomer ratios, and spectroscopic properties as well as published data and computations with other donor sets (Cl^- vs. amine vs. pyridine) were used to validate the various methods. The conclusions are: (1) the choice of method variation (nuclear charge Q on copper or of the amount of HF exchange in the functional) depends on the chromophore (type of donor atoms). (2) With a given chromophore (e.g., Cu^{II}/bispidine/

Cl^-) the choice of method also depends on the problem to be solved (spin distribution; covalency of the copper–donor interaction; structure; isomer distribution; spectroscopy). (3) Solvation is needed to accurately predict isomer ratios. (4) The SORCI method may be used to accurately determine the spin distribution. (5) LF-DFT with a pure DFT functional and a modified nuclear charge Q on copper (where Q is tuned to the SORCI spin distribution) leads to accurately predicted spectroscopic parameters. Alternatively, a tuned hybrid functional with added HF exchange and $Q = 29$ on copper may also be used. The determination of spectroscopic parameters by SORCI calculations needs a large reference space.

The not unexpected (but somewhat frustrating) conclusion is that semiempirical methods (DFT with tuned hybrid functionals or a variation of the nuclear charge of the metal center) need to be optimized for each type of compound and for each molecular property.

References

1. Siegbahn, P. E. M.; Blomberg, M. R. A. Chem Rev 2000, 100, 421.
2. Friesner, R. A.; Dunietz, B. D. Acc Chem Res 2001, 34, 351.
3. Siegbahn, P. E. M. J Comp Chem 2001, 22, 1634.
4. Koch, W.; Holthausen, M. C. A Chemist's Guide to Density Functional Theory, John Wiley & Sons, Inc.: Chichester, UK, 2001, 2nd ed.
5. Basumallick, L.; Sarangi, R.; DeBeer, G. S.; Elmore, B.; Hooper, A. B.; Hedman, B.; Hodgson, K. O.; Solomon, E. I. J Am Chem Soc 2005, 127, 3531.
6. Siegbahn, P. E. M.; Blomberg, M. R. A.; Wirstam nee Pavlov, M.; Crabtree, R. H. J Biol Inorg Chem 2001, 6, 460.
7. Szilagyi, R. K.; Metz, M.; Solomon, E. I. J Phys Chem A 2002, 106, 2994.
8. Koszinowski, K.; Schoeder, D.; Schwarz, H.; Holthausen, M. C.; Sauer, J.; Soizumi, H.; Armentrout, P. B. Inorg Chem 2002, 41, 5882.
9. Schatz, M.; Raab, V.; Foxon, S.; Brehm, G.; Schneider, S.; Reiher, M.; Holthausen, M. C.; Sundermeyer, J.; Schindler, S. Angew Chem, Int Ed 2004, 43, 4360.
10. Siegbahn, P. E. M.; Crabtree, R. H. Structure and Bonding; Springer-Verlag: Berlin, 2000.
11. Himo, F.; Siegbahn, P. E. M. J Am Chem Soc 2001, 123, 10280.
12. Holthausen, M. C. J Comp Chem 2005, 26, 1505.
13. DeBeer George, S.; Basumallick, L.; Szilagyi, R. K.; Randall, D. W.; Hill, M. G.; Nersissian, A. M.; Valentine, J. S.; Hedman, B.; Hodgson, K. O.; Solomon, E. I. J Am Chem Soc 2003, 125, 11314.
14. Becke, A. D. J. J Chem Phys B 1993, 98, 5648.
15. Perdew, J. P. Phys Rev B 1986, 33, 8822.
16. Gewirth, A. A.; Cohen, S. L.; Schugar, H. J.; Solomon, E. I. Inorg Chem 1987, 26, 1933.
17. Didziulis, S. V.; Cohen, S. L.; Gewirth, A. A.; Solomon, E. I. J Am Chem Soc 1988, 110, 250.
18. Deeth, R. J. J Chem Soc, Dalton Trans 2001, 664.
19. Comba, P.; Kerscher, M.; Merz, M.; Müller, V.; Pritzkow, H.; Remenyi, R.; Schiek, W.; Xiong, Y. Chem Eur J 2002, 8, 5750.
20. Comba, P.; Schiek, W. Coord Chem Rev 2003, 238–239, 21.
21. Comba, P.; Kerscher, M. Cryst Eng 2004, 6, 197.
22. Comba, P.; Hauser, A.; Kerscher, M.; Pritzkow, H. Angew Chem Int Ed 2003, 42, 4536.
23. Comba, P.; Martin, B.; Prikhod'ko, A.; Pritzkow, H.; Rohwer, H. Comptes Rendus Chimie 2005, 6, 1506.
24. Comba, P.; Lopez de Laorden, C.; Pritzkow, H. Helv Chim Acta 2005, 88, 647.
25. Bleiholder, C.; Börzel, H.; Comba, P.; Ferrari, R.; Heydt, A.; Kerscher, M.; Kuwata, S.; Laurenczy, G.; Lawrance, G. A.; Lienke, A.; Martin, B.; Merz, M.; Nuber, B.; Pritzkow, H. Inorg Chem 2005, 44, 8145.
26. Born, K.; Comba, P.; Ferrari, R.; Lawrance, G. A. in preparation.
27. Comba, P.; Merz, M.; Pritzkow, H. Eur J Inorg Chem 2003, 1711.
28. Börzel, H.; Comba, P.; Katsichtis, C.; Kiefer, W.; Lienke, A.; Nagel, V.; Pritzkow, H. Chem Eur J 1999, 5, 1716.
29. Börzel, H.; Comba, P.; Hagen, K. S.; Katsichtis, C.; Pritzkow, H. Chem Eur J 2000, 6, 914.
30. Comba, P.; Lienke, A. Inorg Chem 2001, 40, 5206.
31. Börzel, H.; Comba, P.; Hagen, K. S.; Kerscher, M.; Pritzkow, H.; Schatz, M.; Schindler, S.; Walter, O. Inorg Chem 2002, 41, 5440.
32. Comba, P.; Kerscher, M.; Roodt, A. Eur J Inorg Chem 2004, 23, 4640.
33. Born, K.; Comba, P.; Fuchs, A.; Daubinet, A.; Wadepohl, H. submitted.
34. Wang, D.; Hanson, G. R. J Magn Reson A 1995, 117, 1.
35. Wang, D.; Hanson, G. R. Appl Magn Reson 1996, 11, 401.
36. Frisch, M. J.; Trucks, G. W.; Schlegel, H. B.; Scuseria, G. E.; Robb, M. A.; Cheeseman, J. R.; Montgomery, J. A., Jr.; Vreven, T.; Kudin, K. N.; Burant, J. C.; Millam, J. M.; Iyengar, S. S.; Tomasi, J.; Barone, V.; Mennucci, B.; Cossi, M.; Scalmani, G.; Rega, N.; Petersson, G. A.; Nakatsuji, H.; Hada, M.; Ehara, M.; Toyota, K.; Fukuda, R.; Hasegawa, J.; Ishida, M.; Nakajima, T.; Honda, Y.; Kitao, O.; Nakai, H.; Klene, M.; Li, X.; Knox, J. E.; Hratchian, H. P.; Cross, J. B.; Bakken, V.; Adamo, C.; Jaramillo, J.; Gomperts, R.; Stratmann, R. E.; Yazyev, O.; Austin, A.; Cammi, R.; Pomelli, C.; Ochterski, J. W.; Ayala, P. Y.; Morokuma, K.; Voth, G. A.; Salvador, P.; Dannenberg, J. J.; Zakrzewski, V. G.; Dapprich, S.; Daniels, A. D.; Strain, M. C.; Farkas, O.; Malick, D. K.; Rabuck, A. D.; Raghavachari, K.; Foresman, J. B.; Ortiz, J. V.; Cui, Q.; Baboul, A. G.; Clifford, S.; Cioslowski, J.; Stefanov, B. B.; Liu, G.; Liashenko, A.; Piskorz, P.; Komaromi, I.; Martin, R. L.; Fox, D. J.; Keith, T.; Al-Laham, M. A.; Peng, C. Y.; Nanayakkara, A.; Challacombe, M.; Gill, P. M. W.; Johnson, B.; Chen, W.; Wong, M. W.; Gonzalez, C.; Pople, J. A.; Gaussian Inc.: Wallingford, CT, 2004.
37. Neese, F. J Chem Phys 2003, 119, 9428.
38. Neese, F. Int J Quantum Chem 2001, 83, 104.
39. Berces, A.; Bo, C.; Boerrigter, P. M.; Cavallo, L.; Chong, D. P.; Deng, L.; Dickson, R. M.; Ellis, D. E.; Fan, L.; Fischer, T. H.; Fonseca Guerra, C.; van Gisbergen, S. J. A.; Groeneveld, J. A.; Gritsenko, O. V.; Grüning, M.; Harris, F. E.; van den Hoek, P.; Jacobsen, H.; van Kessel, G.; Kootstra, F.; van Lenthe, E.; McCormack, D. A.; Osinga, V. P.; Patchkovskii, S.; Philipsen, P. H. T.; Post, D.; Pye, C. C.; Ravenek, W.; Ros, P.; Schipper, P. R. T.; Schreckenbach, G.; Snijders, J. G.; Sola, M.; Swart, M.; Swerhone, D.; te Velde, G.; Vernooijs, P.; Versluis, L.; Visser, O.; van Wezenbeek, E.; Wiesenekker, G.; Wolff, S. K.; Woo, T. K.; Baerends, E. J.; Autschbach, J.; Ziegler, T. ADF2004.01; SCM, Theoretical Chemistry, Vrije Universiteit: Amsterdam, The Netherlands, 2004; http://www.scm.com.
40. te Velde, G.; Bickelhaupt, F. M.; Baerends, E. J.; Fonseca Guerra, C.; van Gisbergen, S. J. A.; Snijders, J. G.; Ziegler, T. J Comp Chem 2001, 22, 931.
41. Atanasov, M.; Daul, C. A.; Rauzy, C. Struct Bond 2004, 106, 97.
42. Mulliken, R. S. J Chem Phys 1955, 23, 1833.
43. Reed, A. E.; Curtiss, L. A.; Weinhold, F. Chem Rev 1988, 88, 899.
44. Bader, R. F. W. Atoms in Molecules: A Quantum Theory; Oxford University Press: Oxford, 1990.
45. Schaefer, A.; Horn, H.; Ahlrichs, R. J Chem Phys 1992, 97, 2571.
46. Weigand, F.; Haeser, M. Theor Chem Acc 1997, 97, 331.
47. Frenking, G.; Wichmann, K.; Fröhlich, N.; Loschen, C.; Lein, M.; Frunzke, J.; Rayon, V. M. Coord Chem Rev 2002, 21, 3351.
48. Szabo, A.; Kovacs, A.; Frenking, G. Z Anorg Allg Chem 2005, 631, 1803.
49. Morokuma, K. J Chem Phys 1971, 55, 1236.

50. Ziegler, T.; Rauk, A. Theor Chim Acta 1977, 46, 1.
51. Neese, F. J Chem Phys 2001, 115, 11080.
52. Reinen, D.; Atanasov, M.; Lee, S. Coord Chem Rev 1998, 175, 91.
53. Wiersema, A. J.; Windle, J. J. J Phys Chem, 68, 2316.
54. Bertrand, P. Inorg Chem 1993, 32, 741.
55. Atkins, P. W.; Symons, M. C. R. The Structure of Inorganic Radicals; Elsevier: Amsterdam, 1967.
56. Comba, P.; Hambley, T. W.; Hitchman, M. A.; Stratemeier, H. Inorg Chem 1995, 34, 3903.
57. McGarvey, B. R. J Phys Chem 1967, 71, 51.
58. Neese, F. J Phys Chem A 2001, 105, 4290.
59. Munzarova, M.; Kaupp, M. J Phys Chem 1999, 103, 9966.
60. Munzarova, M.; Kubacek, P.; Kaupp, M. J Am Chem Soc 2000, 122, 11900.
61. Gleiter, R.; Kobayashi, M.; Kuthan, J. Tetrahedron 1976, 32, 2775.
62. Kitaura, K.; Morokuma, K. Int J Quantum Chem 1976, 10, 325.
63. Comba, P.; Hambley, T. W.; Okon, N.; Lauer, G. MOMEC97, a Molecular Modeling Package for Inorganic Compounds; Heidelberg, 1997.
64. Bol, J. E.; Buning, C.; Comba, P.; Reedijk, J.; Ströhle, M. J Comput Chem 1998, 19, 512.
65. Perdew, J. P.; Burke, K.; Ernzerhof, M. Phys Rev Lett 1996, 77, 3865.
66. Perdew, J. P. Phys Rev Lett 1996, 78, 1396.
67. Neese, F. Magn Reson Chem 2004, 42, 187.
68. Atanasov, M.; Baerends, E. J.; Baettig, P.; Daul, C.; Rauzy, C.; Zbiri, M.; Chem Phys Lett 2004, 399, 433.